Deep learning-based molecular dynamics simulation reconfiguration of efficient heat energy transport of Gra/h-BN heterointerface

View Online   Export Citation   CrossMark

Haiying Yang,[1,2,a] Lin Li,[1] and Ping Yang[1,a] (iD)

AFFILIATIONS

[1]Laboratory of Advanced Design, Manufacturing & Reliability for MEMS/NEMS/OEDS, School of Mechanical Engineering, Jiangsu University, Zhenjiang 212013, People's Republic of China
[2]School of Materials Engineering, Purdue University, West Lafayette, Indiana 47907, USA

[a]Authors to whom correspondence should be addressed: haiyingyang 99@163.com and yangpingdm@ujs.edu.cn

ABSTRACT

We investigate the reconfiguration scheme of efficient heat energy transport of the Gra/h-BN heterointerface by a hybrid enhanced machine learning method combining an integrated iterative method, automatic modeling, non-equilibrium molecular dynamics calculation, and convolutional neural network (CNN). The results show that the method identifies the optimal defect distribution in gra/h-BN from tens of millions of possible defect configurations, and the interfacial thermal conductivity (ITC) of the vdW gra/h-BN heterointerface in the optimal defect distribution is 97% higher than that in the original gra. Furthermore, the heat transfer transformation of the vdW gra/h-BN heterointerface with different defect distributions at room temperature can be observed efficiently. The dependency law between the defect distribution and the ITC is revealed by combining the CNN model of the ResNet network. The efficient heat energy transport design can promote the sustainable service life of materials and structures.

Studies indicate that for every 10–15 °C rise in the temperature of electronic components, their lifespan diminishes by approximately 50%.[1,2] Graphene (gra) is known for its extraordinary in-plane thermal conductivity. However, the heat dissipation efficiency in graphene-based devices is often limited by the interfacial thermal resistance (ITR) between graphene and substrate materials.[3–7] Hexagonal boron nitride (h-BN), an insulator possessing atomically flat surfaces and lacking dangling bonds and electrical traps, shares a similar lattice constant with gra. This feature facilitates their vertical integration, forming a high-quality heterointerface and thereby positioning h-BN as an optimal substrate for gra.[8–15] To minimize the thermal resistance at the interface of a 2D van der Waals heterointerface, various strategies are employed, including defect introduction, doping, interlayer rotation, and functional modifications.[16–33] Therefore, precise control of the types and distribution of defects is crucial in order to obtain a gra/h-BN structure with high thermal conductivity. Machine learning has been employed to predict the mechanical properties of gra, taking into account numerous factors such as temperature, strain rate, vacancy defects, chirality, etc.[34–40] Although these studies have provided valuable methods for optimizing the thermal properties of materials, they mostly focus on a single type of defect or specific interface parameters.

In this study, we introduce an iterative, evolutionary approach that integrates automated modeling using Python, MD computations, and optimization via a convolutional neural network (CNN) algorithm to engineer an optimal gra/h-BN heterointerface to improve thermal conduction. We applied non-equilibrium molecular dynamics (NEMD) simulations across numerous vdW gra/h-BN heterointerfaces at ambient conditions, each featuring unique defect patterns. The relationship between defect distribution patterns and interfacial thermal conductance was explored using a convolutional neural network algorithm modified by a Residual Network (ResNet). This systematic investigation identified the most effective defect distribution from tens of millions of potential gra/h-BN configurations, resulting in significantly increased thermal conduction efficiency compared to pristine graphene.

Figures 1(a1) and 1(a2) shows the temperature distribution of the pristine gra/h-BN interface after reaching a non-equilibrium steady state. Each data point corresponds sequentially to the statistical temperature of each layer. By averaging the input power in the cold region
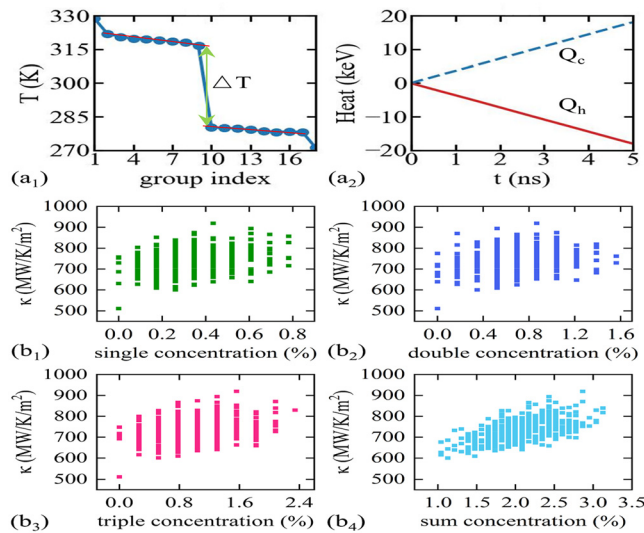
FIG. 1. (a_1) Temperature distribution of the pristine gra/h-BN. (a_2) The change in energy accumulation of the heat source Q_h and heat sink Q_c. (b_1)–(b_4) The ITC distribution statistics at various concentrations for single-point, double-point, triple-point, and overall defects in the 300 initial datasets.

and the output power in the hot region in Fig. 1(a_2), we can obtain the heat flow density J,

$$J = \frac{1}{A} \frac{Q_h + Q_c}{2\Delta t}, \tag{1}$$

where Q_c and Q_h represent the cumulative energy in the cold and hot regions (the heat sink and heat source areas) over the operation time Δt, and A represents the axial effective heat transfer area. Therefore, at a temperature of 300 K, using Eq. (1), we derive the interfacial thermal conductivity (ITC) of the gra/h-BN interface to be 511 ± 12 MWm^{-2}K^{-1}. Table I shows the results are close to simulation results by Ren[22] and Wu.[41] However, there is a significant difference compared to the DFT results of Mao.[42] Moreover, an even more pronounced discrepancy exists when comparing with the experimental results obtained by Chen[43] through Raman spectroscopy, which is 7.41 ± 0.43 MWm^{-2}K^{-1}. To verify whether the scale of the simulation

TABLE I. Comparison of several results.

	Refs.	Method	κ (MWm^{-2}K^{-1})
Exp	Chen et al.[43]	Raman spectroscopy	7.41 ± 0.43
Theory	Mao et al.[42]	Density functional theory	186 ± 7
Simulation	Ren et al.[22]	NEMD with $A = 95$ nm^2	509 ± 25
	Wu et al.[42]	NEMD with $A = 6.25$ nm^2	300 ± 12
	This work	NEMD with $A = 25$ nm^2	511 ± 21

system is appropriate, we constructed 300 gra/h-BN interface models with different defect distributions, calculated the ITC values, and conducted convergence tests.

Figures 1(b1)–1(b4) shows a statistical analysis of the impact of the single-point, double-point, triple-point, and overall defect concentrations on the ITC in the 300 initial datasets. We considered three main types of point defects; the detailed atomic structures of these defect types can be viewed in Fig. S1 of the supplementary material. In Figs. 1(b1)–1(b3), the ITC generally shows a trend of first increasing and then decreasing with the concentration of each type of defect, with the peak ITC always at the median concentration position. It can be inferred that when the three types of defects in gra coexist and the number of defects is uniform, it has a positive effect on the enhancement of ITC. In Fig. 1(b4), the thermal conductivity first increases and then decreases with the sum of all types of defects, and the inflection point appears at a larger total concentration.

Figure 2 provides a detailed depiction of the results from the first five trials of using Optuna for CNN hyperparameter optimization, which involved training on the initial 300 datasets. Trial 1 in Fig. 2(a) shows that when the hyperparameters remain unchanged, mean squared error (MSE) converges at a high level, preventing CNN from obtaining a high precision. In Figs. 2(a) and 2(b), as the number of trials increases and as the CNN is configured with different combinations of hyperparameters, the overall MSE value of the training rapidly decreases, further exhibiting a trend toward convergence. This validates that our Optuna hyperparameter search process is both effective and stable. Figures 3(a_1)–3(b_3) demonstrate the distribution of the highest ITC defects of gra obtained in each iteration and the prediction error of the CNN model. Figure 3(a_1) shows the initial 300 datasets present a wide distribution of ITC, reaching a maximum value of 889.21 MWm^{-2}K^{-1}. However, due to the limitations of the small training set, the understanding ability of the CNN is inadequate for the configuration–ITC relationship, leading to a large error between its predicted ITC and the results calculated by MD. The RMSE and MAPE are 48.8 MWm^{-2}K^{-1} and 6.93%, respectively. As the number of iterations increases, the CNN gradually learns more data, and the prediction accuracy steadily improves. By the fifth iteration, the RMSE and MAPE have dropped to 8.42 MWm^{-2}K^{-1} and 1.32%, respectively, achieving more accurate predictions within a wide ITC range of 500–1000 MWm^{-2}K^{-1}, validating the ability of the CNN to extract the feature of gra defect configuration space. Figures 3(a2) and 3(a3) shows the newly added datasets are mainly concentrated in the high ITC area (greater than 800 MWm^{-2}K^{-1}), because each additional dataset is derived from the top 100 high ITC configurations predicted by the CNN in the previous iteration, which effectively enhances the directionality of the prediction for optimal ITC. After five iterations, the CNN prediction met the preset accuracy conditions and found the distribution configuration of the highest ITC defects in Fig. 3(b_3), with an ITC value of 1004.69 MWm^{-2}K^{-1}. Figure 3(b_3) shows the concentrations of various types of defects are not evenly distributed (single defect > triple defect > double defect), which is different from the initial conjecture that high ITC configurations in the 300 random datasets were evenly distributed in defect types. This validates that the data-driven evolutionary CNN prediction model obtained information beyond the initial dataset during the iterative process, breaking our original artificial inference. Compared with the pristine gra structure, the optimal configuration designed by our evolutionary CNN has improved the ITC by 97%.
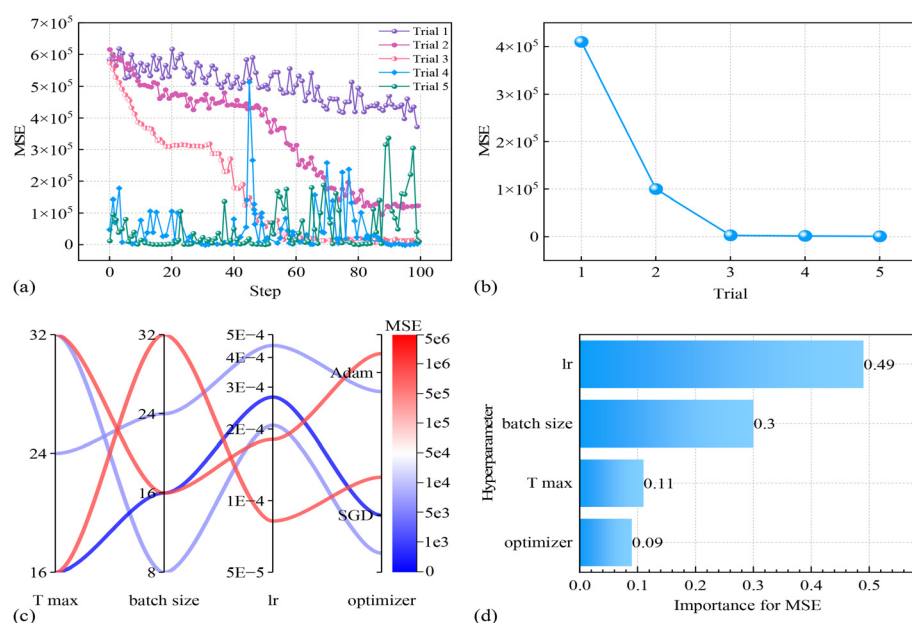
FIG. 2. The results of Optuna optimizing the hyperparameters of the CNN. (a) The relationship between the MSE and step for different trials. (b) The relationship between MSE and overall trial variation in Optuna. (c) High-dimensional hyperparameter relationship graph. (d) The importance of hyperparameters to MSE.
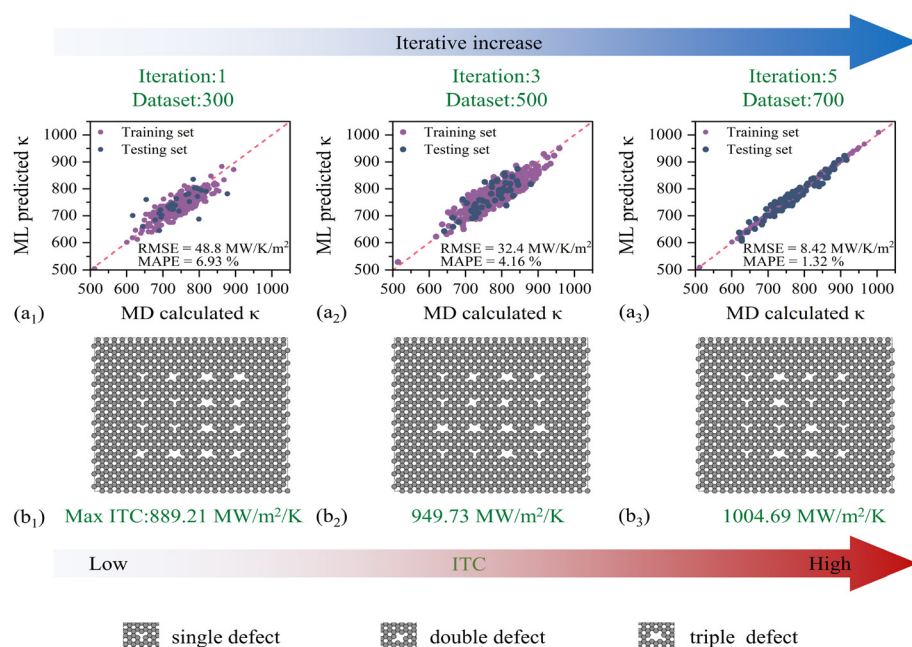

FIG. 3. (a) The root mean square error (RMSE) and mean absolute percentage error (MAPE) of the train set and the test set change with the increase in iterations. The subscripts 1, 2, and 3 represent the results of the 1st, 3rd, and 5th iterations, respectively, with training data sizes of 300, 500, and 700, respectively. (b_1)–(b_3) The top views of the defects distribution of maximum ITC found after the 1st, 3rd, and 5th iterations. Defect type labels have been added below.

A hybrid design method combining an integrated iterative method, automatic modeling, non-equilibrium molecular dynamics (NEMD) calculation, and convolutional neural network (CNN) training is proposed to investigate the ITC of the gra/h-BN interface. We elucidate the profound impact of mixed defect distributions on the thermal performance of gra/h-BN interfaces. Given identical defect concentrations, pronounced alterations in ITC have been unveiled via NEMD calculations. Implementing an iterative CNN methodology, we have trained an array of defect configurations, enabling the discovery of an optimal configuration within a 3^{16} design space. The ITC of the optimized gra/h-BN model recorded a significant boost, reaching 1004.69 MWm^{-2}K^{-1} - an escalation of 97% compared to its original pristine form, underlining the efficacy and precision of the iterative CNN approach in determining optimal structures. Our research also emphasizes the significance of optimal hyperparameter selection in machine learning-based materials research. This investigation substantiates the capability of machine learning in unearthing optimal physical attribute representations, independent of human preconceptions.

19 July 2025 05:41:28

Ultimately, this study offers fresh insights into the crucial role defect distribution plays in thermal conduction, thus advancing the integration of data mining within micro/nano manufacturing. In forthcoming research endeavors, the adoption of this intelligent convolutional neural network methodology will enable the investigation of thermal characteristics in an expanded range of micro- and nanoscale structures.

See the supplementary material for the method of this paper and supporting information for deep learning-based molecular dynamics simulation reconfiguration of efficient heat energy transport of the Gra/h-BN heterointerface.

AUTHOR DECLARATIONS

Conflict of Interest

The authors have no conflicts to disclose.

Author Contributions

Haiying Yang: Conceptualization (lead); Investigation (equal); Methodology (equal). **Lin Li:** Investigation (equal). **Ping Yang:** Resources (lead); Supervision (lead).

DATA AVAILABILITY

The data that support the findings of this study are available from the corresponding authors upon reasonable request.

REFERENCES

[1] K. M. Razeeb, E. Dalton, G. L. W. Cross, and A. J. Robinson, "Present and future thermal interface materials for electronic devices," Int. Mater. Rev. **63**(1), 1–21 (2018).

[2] K. J. Laidler, "The development of the Arrhenius equation," J. Chem. Educ. **61**(6), 494 (1984).

[3] G. Li, J. Zhang, and J. Gao, "Study on structure optimization of a dual IGBT module heat sink in a DC–DC converter under natural convection based on field synergy theory," IEEJ Trans. Electr. Electron. Eng. **14**(10), 1524–1531 (2019).

[4] A. A. Balandin, S. Ghosh, W. Bao, I. Calizo, D. Teweldebrhan, F. Miao, and C. N. Lau, "Superior thermal conductivity of single-layer graphene," Nano Lett. **8**(3), 902–907 (2008).

[5] N. Han, E. Jung, M. Han, B. D. Ryu, K. B. Ko, Y. J. Park, T. Cuong, J. Cho, H. Kim, and C.-H. Hong, "Reduced junction temperature and enhanced performance of high power light-emitting diodes using reduced graphene oxide pattern," J. Phys. D: Appl. Phys. **48**(26), 265102 (2015).

[6] N. Han, T. V. Cuong, M. Han, B. D. Ryu, S. Chandramohan, J. B. Park, J. H. Kang, Y. J. Park, K. B. Ko, H. Y. Kim, H. K. Kim, J. H. Ryu, Y. S. Katharria, C. J. Choi, and C. H. Hong, "Improved heat dissipation in gallium nitride light-emitting diodes with embedded graphene oxide pattern," Nat. Commun. **4**(1), 1452 (2013).

[7] K. S. Novoselov, A. K. Geim, S. V. Morozov, D. Jiang, Y. Zhang, S. V. Dubonos, I. V. Grigorieva, and A. A. Firsov, "Electric field effect in atomically thin carbon films," Science **306**(5696), 666–669 (2004).

[8] C. Lee, X. Wei, J. W. Kysar, and J. Hone, "Measurement of the elastic properties and intrinsic strength of monolayer graphene," Science **321**(5887), 385–388 (2008).

[9] Y. Zhang, V. W. Brar, C. Girit, A. Zettl, and M. F. Crommie, "Origin of spatial charge inhomogeneity in graphene," Nat. Phys. **5**(10), 722–726 (2009).

[10] C. R. Dean, A. F. Young, I. Meric, C. Lee, L. Wang, S. Sorgenfrei, K. Watanabe, T. Taniguchi, P. Kim, K. L. Shepard, and J. Hone, "Boron nitride substrates for high-quality graphene electronics," Nat. Nanotechnol. **5**(10), 722–726 (2010).

[11] R. Decker, Y. Wang, V. W. Brar, W. Regan, H. Z. Tsai, Q. Wu, W. Gannett, A. Zettl, and M. F. Crommie, "Local electronic properties of graphene on a BN substrate via scanning tunneling microscopy," Nano Lett. **11**(6), 2291–2295 (2011).

[12] M. Wang, S. K. Jang, W. J. Jang, M. Kim, S. Y. Park, S. W. Kim, S. J. Kahng, J. Y. Choi, R. S. Ruoff, Y. J. Song, and S. Lee, "A platform for large-scale graphene electronics–CVD growth of single-layer graphene on CVD-grown hexagonal boron nitride," Adv Mater. **25**(19), 2746–2752 (2013).

[13] C. Zhang, S. Zhao, C. Jin, A. L. Koh, Y. Zhou, W. Xu, Q. Li, Q. Xiong, H. Peng, and Z. Liu, "Direct growth of large-area graphene and boron nitride heterostructures by a co-segregation method," Nat. Commun. **6**(1), 6519 (2015).

[14] F. Withers, O. Del Pozo-Zamudio, S. Schwarz, S. Dufferwiel, P. M. Walker, T. Godde, A. P. Rooney, A. Gholinia, C. R. Woods, P. Blake, S. J. Haigh, K. Watanabe, T. Taniguchi, I. L. Aleiner, A. K. Geim, V. I. Fal'ko, A. I. Tartakovskii, and K. S. Novoselov, "WSe(2) light-emitting tunneling transistors with enhanced brightness at room temperature," Nano Lett. **15**(12), 8223–8228 (2015).

[15] J. Bao, M. Edwards, S. Huang, Y. Zhang, Y. Fu, X. Lu, Z. Yuan, K. Jeppson, and J. Liu, "Two- dimensional hexagonal boron nitride as lateral heat spreader in electrically insulating packaging," J. Phys. D: Appl. Phys. **49**(26), 265501 (2016).

[16] X. Wang and F. Xia, "Van der Waals heterostructures: Stacked 2D materials shed light," Nat. Mater. **14**(3), 264–265 (2015).

[17] H. Yang, S. Gao, Y. Pan, and P. Yang, "Manipulating heat transfer at graphene/silicon interface with nitrogen doping," Int Commun. Heat Mass Transfer **155**, 107521 (2024).

[18] H. Yang, Y. Shen, L. Li, Y. Pan, and P. Yang, "Surface modification to induce efficient heat transfer at graphene/silicon heterointerface," Appl. Therm. Eng. **238**, 121913 (2024).

[19] J. Song, Z. Xu, X. He, C. Cai, Y. Bai, L. Miao, and R. Wang, "Effect of strain and defects on the thermal conductance of the graphene/hexagonal boron nitride interface," Phys. Chem. Chem. Phys. **22**(20), 11537–11545 (2020).

[20] M. Li, B. Zheng, K. Duan, Y. Zhang, Z. Huang, and H. Zhou, "Effect of defects on the thermal transport across the graphene/hexagonal boron nitride interface," J. Phys. Chem. C **122**(26), 14945–14953 (2018).

[21] H. Yang, S. Gao, X. Xu, and P. Yang, "Enhancing heat energy transfer at graphene/polypropylene interface," Appl. Energy **381**, 125134 (2025).

[22] W. Ren, Y. Ouyang, P. Jiang, C. Yu, J. He, and J. Chen, "The impact of interlayer rotation on thermal transport across graphene/hexagonal boron nitride van der Waals heterostructure," Nano Lett. **21**(6), 2634–2641 (2021).

[23] L. Zhang and L. Liu, "Hierarchically hydrogen-bonded graphene/polymer interfaces with drastically enhanced interfacial thermal conductance," Nanoscale **11**(8), 3656–3664 (2019).

[24] X. Xu, Y. Shen, and P. Yang, "Building efficient thermal transport at graphene/polypropylene interfaces by non-covalent functionalized graphene," Phys. Lett. A **469**, 128766 (2023).

[25] L. Liu, M. Qing, Y. Wang, and S. Chen, "Defects in graphene: Generation, healing, and their effects on the properties of graphene: A review," J. Mater. Sci. Technol. **31**(6), 599–606 (2015).

[26] J. C. Meyer, C. Kisielowski, R. Erni, M. D. Rossell, M. F. Crommie, and A. Zettl, "Direct imaging of lattice atoms and topological defects in graphene membranes," Nano Lett. **8**(11), 3582–3586 (2008).

[27] M. H. Gass, U. Bangert, A. L. Bleloch, P. Wang, R. R. Nair, and A. K. Geim, "Free-standing graphene at atomic resolution," Nat. Nanotechnol. **3**(11), 676–681 (2008).

[28] J. Oh, H. Yoo, J. Choi, J. Y. Kim, D. S. Lee, M. J. Kim, J.-C. Lee, W. N. Kim, J. C. Grossman, J. H. Park, S.-S. Lee, H. Kim, and J. G. Son, "Significantly reduced thermal conductivity and enhanced thermoelectric properties of single- and bilayer graphene nanomeshes with sub-10 nm neck-width," Nano Energy **35**, 26–35 (2017).

[29] K. Kim, H. B. Lee, R. W. Johnson, J. T. Tanskanen, N. Liu, M. G. Kim, C. Pang, C. Ahn, S. F. Bent, and Z. Bao, "Selective metal deposition at graphene line defects by atomic layer deposition," Nat. Commun. **5**(1), 4781 (2014).

[30] Y. Lin, J. Pan, H. F. Zhou, H. J. Gao, and Y. Li, "Mechanical properties and optimal grain size distribution profile of gradient grained nickel," Acta Mater. **153**, 279–289 (2018).

[31]B. Mortazavi and S. Ahzi, "Thermal conductivity and tensile response of defective graphene: A molecular dynamics study," Carbon **63**, 460–470 (2013).

[32]I. M. Felix and L. F. C. Pereira, "Thermal conductivity of Thue–Morse and double-period quasiperiodic graphene-hBN superlattices," Int. J. Heat Mass Transfer **186**, 122464 (2022).

[33]M. N. Esfahani, M. Jabbari, Y. Xu, and C. Soutis, "Effect of nanoscale defects on the thermal conductivity of graphene," Mater. Today Commun. **26**, 101856 (2021).

[34]Z. Zhang, Y. Hong, B. Hou, Z. Zhang, M. Negahban, and J. Zhang, "Accelerated discoveries of mechanical properties of graphene using machine learning and high-throughput computation," Carbon **148**, 115–123 (2019).

[35]J. L. Beckham, K. M. Wyss, Y. Xie, E. A. McHugh, J. T. Li, P. A. Advincula, W. Chen, J. Lin, and J. M. Tour, "Machine learning guided synthesis of flash graphene," Adv. Mater. **34**(12), e2106506 (2022).

[36]J. Wan, J.-W. Jiang, and H. S. Park, "Machine learning-based design of porous graphene with low thermal conductivity," Carbon **157**, 262–269 (2020).

[37]H. Wei, H. Bao, and X. Ruan, "Genetic algorithm-driven discovery of unexpected thermal conductivity enhancement by disorder," Nano Energy **71**, 104619 (2020).

[38]B. Zheng and G. X. Gu, "Tuning the graphene mechanical anisotropy via defect engineering," Carbon **155**, 697–705 (2019).

[39]M. A. N. Dewapriya, R. K. N. D. Rajapakse, and W. P. S. Dias, "Characterizing fracture stress of defective graphene samples using shallow and deep artificial neural networks," Carbon **163**, 425–440 (2020).

[40]K. T. Butler, D. W. Davies, H. Cartwright, O. Isayev, and A. Walsh, "Machine learning for molecular and materials science," Nature **559**(7715), 547–555 (2018).

[41]X. Wu and Q. Han, "Phonon thermal transport across multilayer graphene/hexagonal boron nitride van der Waals heterostructures," ACS Appl. Mater. Interfaces **13**, 32564–32578 (2021).

[42]R. Mao, B. D. Kong, K. W. Kim, T. Jayasekera, A. Calzolari, and M. Buongiorno Nardelli, "Phonon engineering in nanostructures: Controlling interfacial thermal resistance in multilayer-graphene/dielectric heterojunctions," Appl. Phys. Lett. **101**(11), 113111 (2012).

[43]C.-C. Chen, Z. Li, L. Shi, and S. B. Cronin, "Thermal interface conductance across a graphene/hexagonal boron nitride heterojunction," Appl. Phys. Lett. **104**(8), 081908 (2014).

19 July 2025 05:41:28